MODELLING OF ENGINEERED CEMENTITIOUS COMPOSITE-REPAIRED SUPERELASTIC-SHAPE MEMORY ALLOY REINFORCED SHEAR WALLS

M. Soto[(1)], D. Palermo[(2)]

[(1)] *MASc Candidate, Department of Civil Engineering, York University, Toronto, Canada, sotox19@yorku.ca*
[(2)] *Professor and Vice Dean, Lassonde School of Engineering, York University, Toronto, Canada, dan.palermo.lassonde.yorku.ca*

Abstract

This paper presents numerical analyses of an experimental study where, previously tested, Superelastic-Shape Memory Alloy (SE-SMA) and typical steel-reinforced concrete shear walls are repaired and tested under the same simulated seismic loading. The original steel-reinforced wall was constructed with conventional deformed steel reinforcement in the longitudinal direction of the web and boundary zones, and in the transverse direction for shear reinforcement and buckling-prevention ties. The SE-SMA wall differed by the replacement of the longitudinal steel reinforcement in the boundary regions within the plastic hinge zone with SE-SMA bars, beyond which they were connected to deformed steel reinforcement through mechanical couplers. Both walls were subjected to quasi-static load reversals to failure, which resulted in substantial damage in the plastic hinge zone, including rupturing of longitudinal reinforcing steel bars, and significant cracking and crushing of the concrete in the steel wall and to a lesser degree in the SE-SMA wall. The repair strategy involved the removal of heavily damaged concrete in the plastic hinge zone, replacement of ruptured and buckled steel reinforcement, addition of starter bars at the base of the wall, and casting of Engineering Cementitious Composites (ECC) to replace the removed concrete. Finite Element (FE) models were first developed to simulate the damage experienced in the walls prior to repairing. The models successfully captured the rupturing of the reinforcing bars in the plastic hinge, concrete crushing and severe cracking near the base of the wall. Subsequently, the models were subjected to the repairing method, while carrying forward the residual state of the models from the first analysis. The numerical models were subjected to the same loading protocol as implemented in the experimental testing. The numerical results of the repair strategy illustrated that the brittle behavior of conventional concrete in tension and its deformation incompatibility with reinforcing bars, are suppressed by a composite system that integrates the self-centering phenomenon of SE-SMA and the distinctive ductility properties of ECC. The repaired walls exhibited enhanced performance in comparison to the original walls, including higher lateral load capacity and improved damage tolerance via improved post-cracking behavior of the ECC. The repaired steel wall dissipated significant energy, while the repaired SE-SMA wall was capable of recovering lateral displacements beyond 2.5% drift.

Keywords: Nonlinear Modelling; Shear Walls; Repair; Engineered Cementitious Composites (ECC); Shape Memory Alloy (SMA)

1. Introduction

Ductility capacity and energy dissipation are two primary characteristics well-designed reinforced concrete shear walls are expected to exhibit to endure a seismic event [1]. The design target is to guarantee the life safety performance level [2]. The objective is readily realized with the use of conventional construction materials, but the structural performance can be typified by significant residual deformation due to yielding of reinforcement and damage from the response of the concrete [3].

Shape Memory Alloys (SMA) are an ideal option for a ductile structure owing to their ability to return to their original shape after apparent plastic deformation (6-8% of strain) once unloaded at room temperature or through a heating process [4]. These exceptional effects are called memory of elastic form (superelasticity) and memory of thermal form (shape memory effect) [5]. Nickel-Titanium (Nitinol) alloy is the most common type of SMA. A recent study illustrated that the substitution of conventional longitudinal reinforcement by Superelastic-Shape Memory Alloy (SE-SMA) in the plastic hinge of a shear wall resulted in greater re-centering capacity and less residual displacements with a sustained drift capacity of 3% prior failure [6] Similarly, ECC is classified as a High-Performance-Fiber Reinforced Cement Composite (HPFRCC) that has

applicability in earthquake design for structures subjected to cyclic load [7] and impact load [8]. This innovative concrete consists of a mortar base matrix comprised of sand, silica fume, cement, fly ash along with 2% volumetric fraction of Polyvinyl Alcohol (PVA) fibers [9]. The tensile capacity varies from 4 to 6 MPa, with large strain capacity between 3% to 5%, exhibiting high ductility by optimizing the microstructure of the composite [10]. The combination of these two innovative materials leads to self-centering with improved damage tolerance [11]. Both SMA and HPFRCC provides an opportunity to improve the impact load capacity and post-earthquake state of the structure, while achieving the design objective and reducing repair costs [12, 13]. It was illustrated that using Ni-Ti reinforcing bars and HPFRC in the plastic hinge region of a column under compression and cyclic lateral loading lead to a displacement ductility greater than 4, where for drift ratios below 3%, the column recovered to 0.5% average residual drift with enhanced crack-closure capability [14].

The literature provides several studies examples on modelling the response of reinforced structures with SE-SMA [15,16]. However, research on simulating the behavior of hybrid SMA-ECC structures is lagging. The paper herein explores numerically the seismic behavior of a shear wall repaired by replacing conventional steel and concrete with SE-SMA and ECC, respectively, in the plastic hinge region.

2. Description of Specimens

The structures investigated as part of this study correspond to two reinforced concrete, ductile shear walls, previously tested by Morcos and Palermo [15], meant to investigate the self-centering capacity of SE-SMA reinforced concrete shear walls. The walls were designed based on the seismic provisions of the Canadian Standards Association (CSA) A23.3 [17, 18]. The original steel-reinforced wall denoted as SWS was constructed with conventional deformed steel reinforcement in the longitudinal direction of the web and boundary zones, and in the transverse direction for shear reinforcement and buckling-prevention ties. The SE-SMA wall designated as SWN differed by the replacement of the longitudinal steel reinforcement in the boundary regions within the plastic hinge zone with SE-SMA bars. The nominal dimensions are identical for both walls as depicted in Fig. 1. The walls have a rectangular cross-section: 150 mm in thickness and 1000 mm in length. The height of the walls is 2200 mm, resulting in an aspect ratio of 2.2, selected to promote a ductile flexural response. Furthermore, these walls were constructed on a 1700 mm-long, 500 mm-high and 1000 mm-wide foundation blocks. The top is capped with a stiff 400 mm by 400 mm beam that measures 1600 mm in length. For Wall SWS, each boundary contains four-10M (100 mm^2 area) longitudinal bars, and the web has total of six, evenly spaced 10M longitudinal bars. The same approach was followed for Wall SWN, except for the conventional longitudinal steel reinforcement in the boundary zones that was replaced with SE-SMA smooth bars with a diameter of 12.7 mm, as illustrated in Fig. 1. The SE-SMA bars were limited to 900 mm within the height of the plastic hinge region and extended 300 mm into the foundation block.

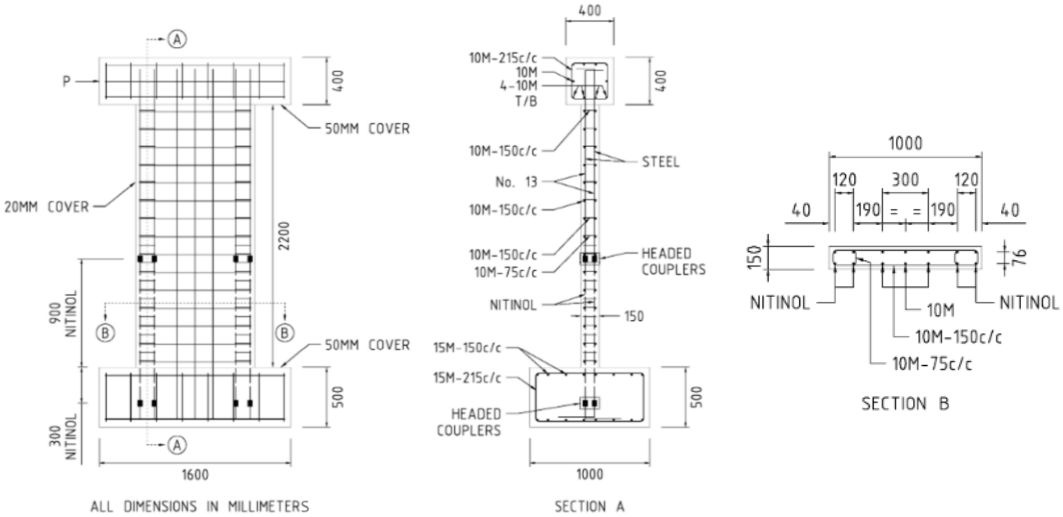

Fig. 1 - Reinforcement details for Wall SWN [15]

2.1 Previous Damage and Visual Inspection

The two original walls were tested under reverse cyclic loading to simulate the effects of a seismic event following a loading protocol established by FEMA 461 [18], in which gradual increments of drift were applied to failure as illustrated in Fig. 2.

Prior to failure, Wall SWN sustained a drift capacity exceeding 5%. Meanwhile, Wall SWS failed at 3% drift [16]. Both walls experienced widespread damage, presenting hairline-flexural cracks above the plastic hinge region. Moreover, the concrete located in the plastic hinge region was severely deteriorated with the development of significant flexural and shear cracks. Fig. 2 (a) illustrates the base of Wall SWS, where severe concrete spalling and crushing arose. In addition, the longitudinal reinforcing bars in the boundary regions ruptured. Likewise, Wall SWN, shown in Fig. 2 (b), developed significant flexural-shear cracks where one major crack was observed approximately 300 mm above the base of the wall. No SE-SMA bar ruptured in the boundary region, however, longitudinal steel reinforcement in the web region ruptured. Furthermore, Wall SWN experienced milder concrete spalling with reduced cracking, attributed to the smooth surface of the SMA bars, which reduced bonding to the surrounding concrete, resulting in fewer but wider cracks. A main difference was observed in the substantial crack along the base of Wall SWN promoting rocking/sliding during testing [16].

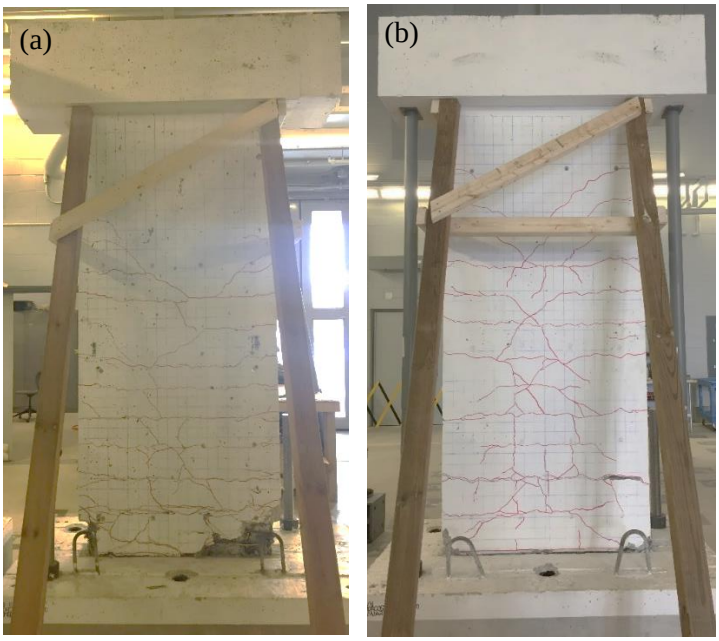

Fig. 2 - Condition of the original walls after testing: (a) SWS; (b) SWN

3. Experimental Program

A general repair procedure was adopted, aiming for a full recovery and strengthening of the walls. The critical deterioration experienced by the walls within the plastic hinge region, and the opportunity to establish a consistent comparison, led to an identical repair procedure in both walls. The method employed followed a chronological order: (1) visual inspection of the previously damaged walls to assess their state and assembly of a bracing system to restrict movement of the walls during the removal of the concrete; (2) replacement of damaged reinforcing bars; (3) formwork construction and assembly; and (4) casting of the ECC where the original concrete was removed.

The heavily damaged concrete at the base of the plastic hinge zone was entirely removed to further investigate the local damage. Wall SWS presented in Fig. 3 (a) experienced rupturing of the deformed steel reinforcing bars in the boundary region of the plastic hinge. Moreover, buckling of the steel bars was evident in the web

zone. Fig. 3 (b) illustrated that Wall SWN experienced no apparent damage to the SE-SMA bars. However, the longitudinal steel reinforcing bars located in the web region ruptured.

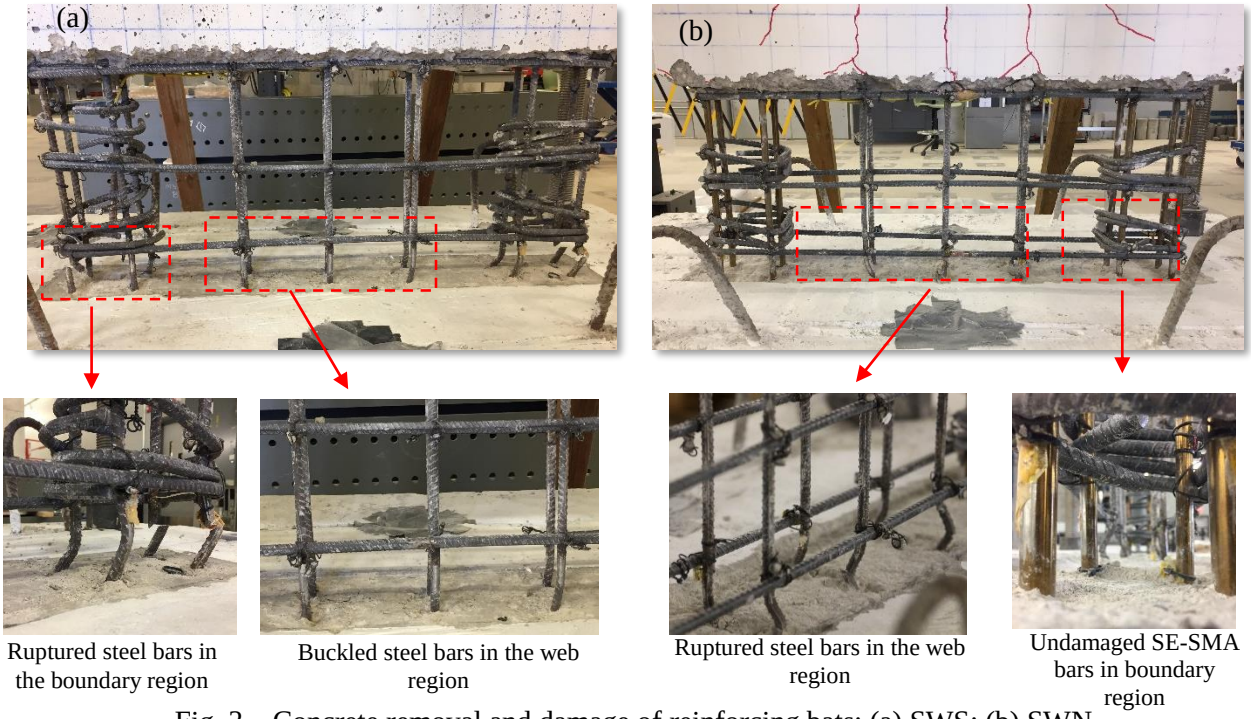

Fig. 3 – Concrete removal and damage of reinforcing bats: (a) SWS; (b) SWN

All ruptured and buckled bars were replaced with new 10M mild-steel deformed bars. The new reinforcing bar segments were connected to the remaining deformed reinforcement with mechanical couplers. In addition, starter bars were installed at the base of the wall to suppress the rocking/sliding presented during the original testing of the SMA wall.

A total of 34 strain gauges were installed at strategic locations in each wall where the damage is expected to be substantial with the objective to record the response of the reinforcing bars. Fig. 4 and Fig. 5 provide the condition of the walls with the replaced reinforcement, starter bars, additional couplers and strain gauges, prior to casting of the ECC.

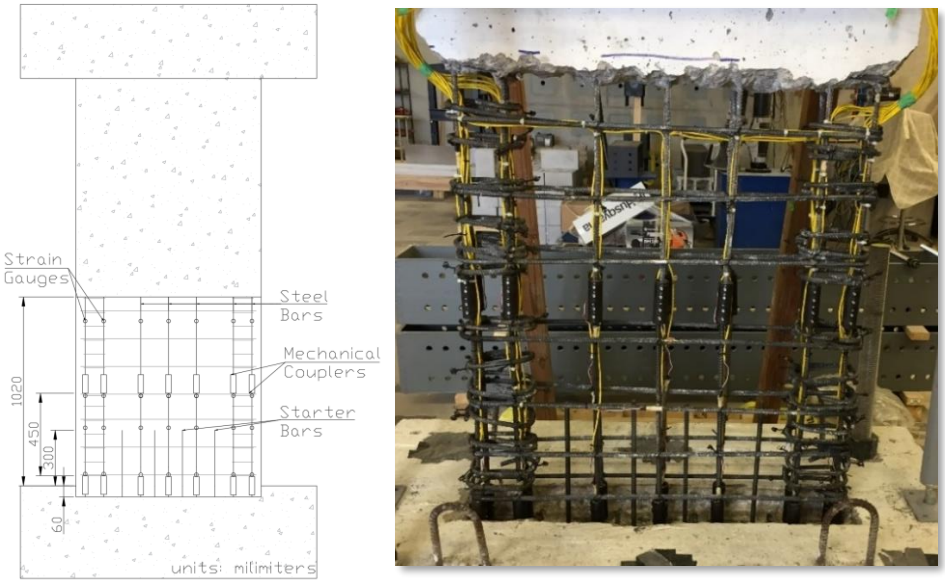

Fig. 4 – Reinforcement layout for SWS-R

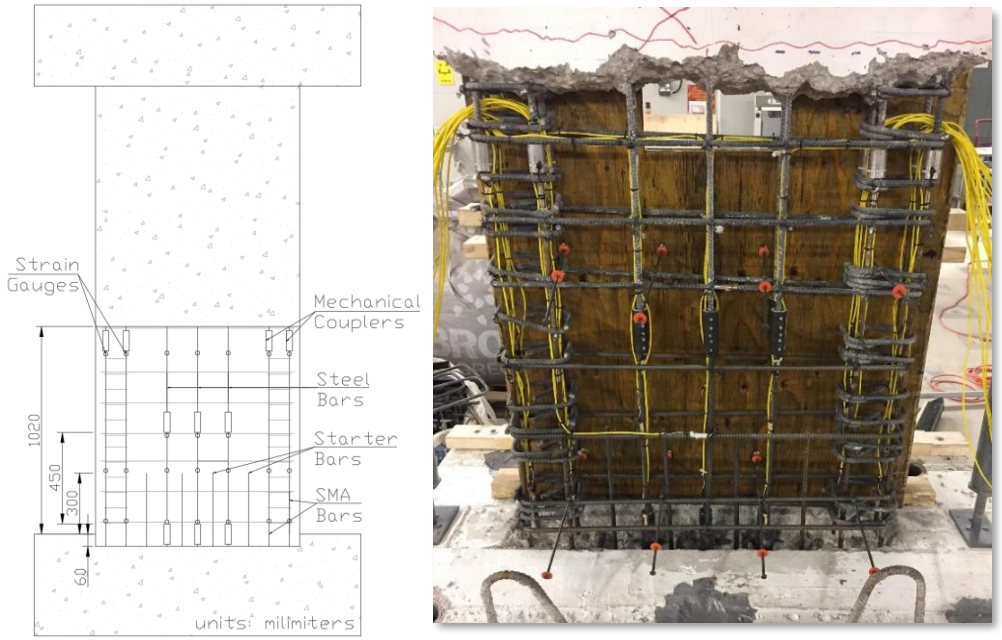

Fig. 5 – Reinforcement layout for SWN-R

Lateral loading, displacements at various locations in the walls and reinforcement strains will be monitored during testing. A set of four steel columns and two steel beams will be assembled to form bracing to control out-of-plane movement during testing. The lateral loading will be imposed with a hydraulic actuator connected to the center of the cap beam at one end and the strong wall at the other end. Cable and linear potentiometers will be employed at different locations to measure displacements, and strain gauges installed on the reinforcement will monitor the strains in the reinforcing bars. The loading protocol will follow that imposed on the original walls. Fig. 6 illustrates the condition of the repaired walls after the repair strategy was completed.

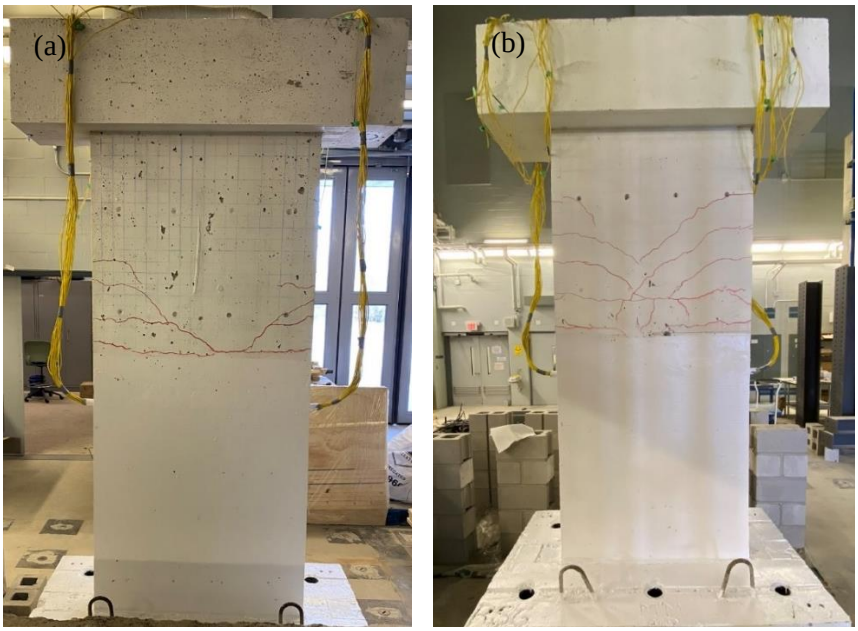

Fig. 6 - Repaired walls: (a) SWS-R; (B) SWN-R

4. Finite Element Models

VecTor2, a two-dimensional nonlinear finite element program was employed to model the walls. The program is based on the Modified Compression Field Theory (MCFT) [19] and the Disturbed Stress Field Model (DSFM) [20]. It is founded on a smeared, rotating crack model for reinforced concrete, in which cracked concrete is represented as an orthotropic material [21]. The software has proven to be an ideal tool for simulating the behavior of reinforced concrete shear walls [23-25].

VecTor2 contains a library of constitutive models for concrete, reinforcement and bond materials that influence the overall response. For the repaired walls of this study, the Popovics-High-Strength Concrete model was selected for the compression pre-peak response of the concrete [25]; it contains a variation of the original Popovics curve that was modified to better reflect the response of concretes with a compressive strength higher than 50 MPa. The post-peak response followed the Modified Park-Kent model [26]. The Kupfer-Richart model was selected to account for the enhancement in the confinement strength in a triaxially compressed concrete [27]. The degradation of strength and stiffness in the cyclic response of the concrete was captured with the Palermo model [28]. Due to the complexity of the matrix composition of ECC, including different types of fibers and the variety of mixtures, most FEM platforms do not contain built-in constitutive models to capture the tensile behavior of this material. The approach taken in VecTor2 involved a custom-input multi-linear response that defines the tensile stress-strain behavior of the ECC as depicted in Fig. 7.

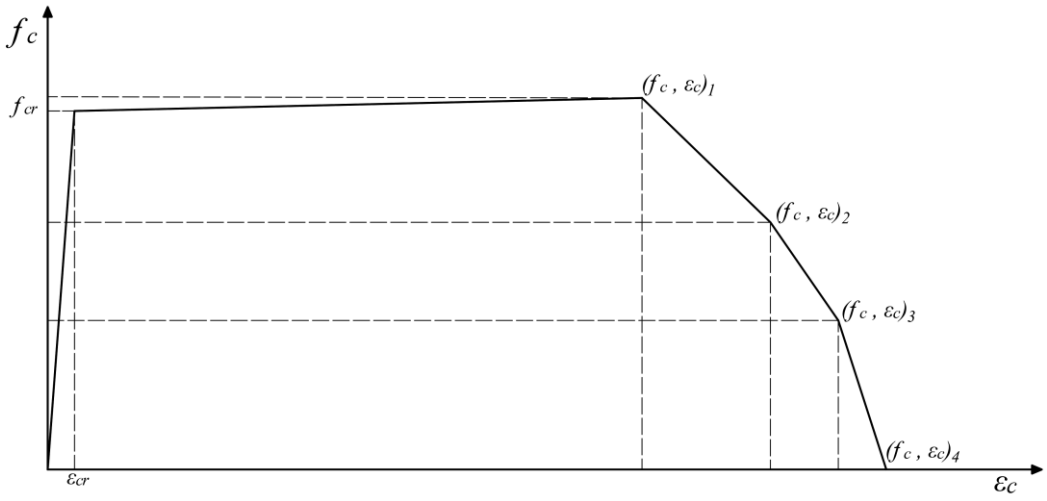

Fig. 7 - Custom-input tensile stress-strain behavior of ECC in VecTor2

Preliminary curve fitting of prism tests was required to obtain the stress-strain data to build the model. The (f_{cr}, ε_{cr}) represents the first crack of the concrete through a linear ascending branch, which marks the initiation of the pseudo strain-hardening tensile behavior of ultra-ductility [29] characterized by multi-cracking. $(f_c, \varepsilon_c)_1$ denotes the peak tensile stress and the completion of the multi-cracking stage. Points $(f_c, \varepsilon_c)_2$, $(f_c, \varepsilon_c)_3$ and $(f_c, \varepsilon_c)_4$ capture the crack localization phase with a strain softening behavior through a trilinear descending branch. Furthermore, second order mechanisms in the concrete behavior, including: dilation and cracking of the concrete followed the default models as recommended by Palermo and Vecchio [30]. Detailed information of the aforementioned models can be found elsewhere [21].

The reinforcing steel followed a typical trilinear response, that includes a linear elastic region, a yield region and a strain hardening zone. The steel hysteresis response was captured with the Seckin model [31]. The Eligehausen model [32] was selected to simulate the bonding mechanism between the concrete and reinforcement. The behavior of the SE-SMA follows a built-in model in VecTor2 and is based on the work of Abdulridha et al. [33] as illustrated in Fig. 8.

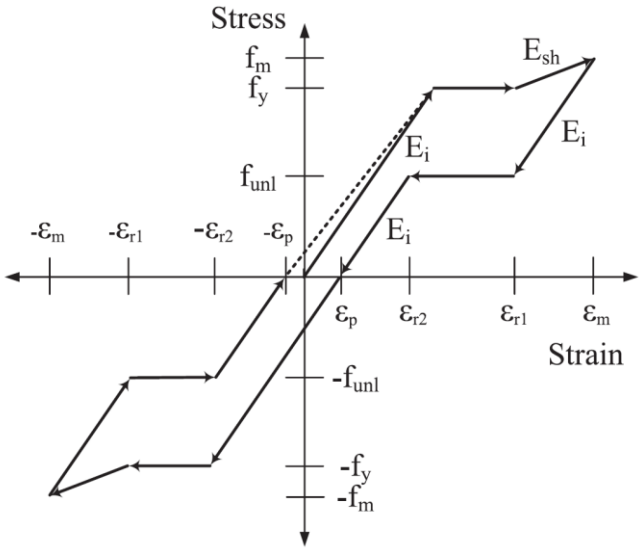

Fig. 8 - SMA plastic offset constitutive model [33]

The model is formed by a series of multi-linear branches representing the hysteresis of SE-Nitinol while being able to capture the self-recovery phenomenon and plastic deformations beyond 6% of strain. The loading phase of the model embodies the transformation from Austenite to Martensite. In the unloading segment, the model simulates the re-transformation to Martensite, capturing the superelasticity.

VecTor2 has the capability to model the chronology of construction of a structure. In addition, the final condition of a stressed structure can be retained and carried forward in the subsequent analysis of the repaired/rehabilitated structure [34]. Two finite element models were developed under this approach: SWS-R and SWN-R. The repaired steel-reinforced wall (SWS-R) served as the companion wall; whereas the repaired SMA-reinforced wall (SWN-R) was evaluated to establish the behavior of an ECC repaired, SE-SMA-reinforced wall. Both analyses served as prediction assessments prior to testing of the wall presented in Fig. 6.

A total of 9 different materials and 8 reinforcement types were employed. The material properties for the analyses herein were adopted from the experimental testing of the original walls (SWS and SWN) reported by Mena and Palermo [15]. Wall SWS had a concrete compressive strength of 47.2MPa, while the reported strength for Wall SWN was 36.9MPa. The concrete in both walls contained a maximum aggregate size of 14mm. The steel reinforcement within wall SWS included 15M bars ($Ø$ = 16mm, F_y = 472.5MPa, and F_u = 578MPa) for the foundation block and 10M bars ($Ø$ =11.3mm, F_y = 454.4MPa, and F_u = 570MPa) for the wall and the cap beam. Wall SWN utilized the same 15M bars for the foundation block. The steel reinforcement for the wall and cap beam was sourced from a different supplier, including 10M bars ($Ø$ = 11.3mm, F_y = 529.4MPa, and F_u = 686.5MPa) and #13 bars ($Ø$ = 12.7mm, F_y = 474.5MPa, and F_u = 639.5MPa). The properties of the SE-SMA bars reported by the manufacturer were: $Ø$ = 12.7mm, F_y = 380MPa and F_u = 900MPa. Finally, the mechanical couplers had the following properties: $Ø$ = 35mm, F_y = 690MPa and F_u = 795MPa. These properties were carried forward into the finite element models of SWS-R and SWN-R.. The ECC repairing material has a compressive strength of 50 MPa and a tensile strength of 6 MPa, with a maximum aggregate size of 0.05 mm and Polyvinyl-Alcohol (PVA) straight-end fibers ($Ø$ = 0.1mm and $Ø$ = 0.04mm). The new segments of 10M bars used to replace the damaged bars have: $Ø$ =11.3mm, F_y = 420MPa, and F_u = 580MPa, while the properties of the mechanical couplers are $Ø$ = 33mm, F_y = 620MPa and F_u = 760MPa.

The construction of both models was similar, 6 subdivisions were required to identify: the web, lower and upper boundary zones, concrete cover and stiff elements (cap beam and foundation block) as presented in Fig. 9. A sensitivity analysis was performed to determine the size of the elements. The mesh size maintained an optimal aspect ratio of 1:1 covering the majority of regions with rectangular elements of 50mm by 50mm, guaranteeing a proper nonlinearity, required to capture the salient features of the structural behavior [30]. Due

to geometric constrains, the concrete cover was the only region that maintained an aspect ratio of 2.5, with 20mm by 50mm elements.

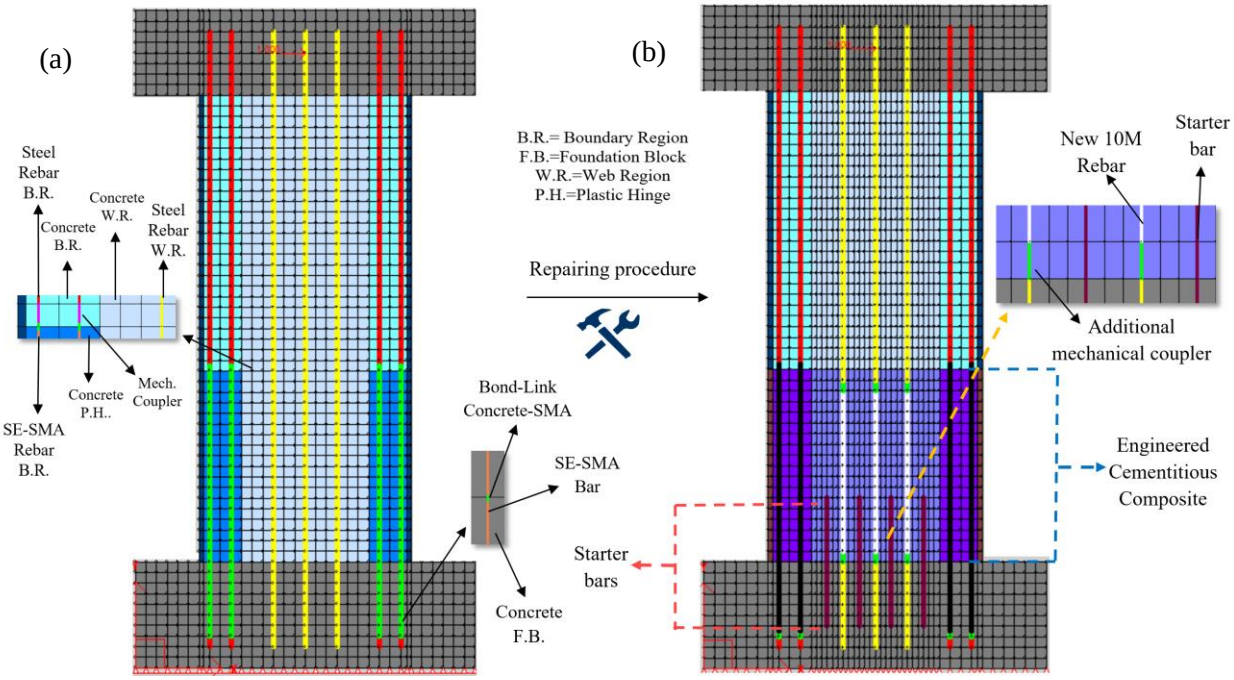

Fig. 9 – FE models: (a) Original wall; (b) Repaired wall

For both models the shear reinforcement and buckling-prevention ties was smeared within the concrete elements. In the web region the reinforcement ratio is 0.89% in the transverse direction. The boundary regions in the plastic hinge zone contain a reinforcement ratio in the transverse direction of 2.67% and an out-of-plane ratio of 1.85% accounting for shear reinforcement and buckling-prevention ties. The top boundary zones, above the plastic hinge region, have 1.78% and 1.11% reinforcement ratio in the transverse and out-of-plane direction, respectively. The concrete cover regions were assumed unreinforced.

The longitudinal reinforcing steel and SE-SMA bars for both walls were modelled as discrete reinforcement, with deformed and smooth truss-bar elements, respectively. The deformed-mild steel was assumed fully bonded to the concrete. Wall SWN-R utilized bond-link elements to represent the interaction between the SE-SMA bars in the plastic hinge with the concrete elements. The mechanical couplers inside the plastic hinge region were modelled with 50mm-long smooth truss-bar elements. The starter bars located at the base of the wall extended 300mm into the plastic hinge, 200mm into the foundation and were simulated as deformed truss-bar elements fully bonded to the concrete. These bars are spaced at 150mm between the web reinforcement.

The loading protocol follows that used by Mena and Palermo [16]. Lateral displacements were applied at an elevation of 2400mm from the base of the wall and at the center of the cap beam. To impose a similar loading protocol, the yield displacement was assumed to be 24mm for both walls, based on results from a previous numerical study on the original walls [15]. As suggested in ATC-24 [35], the loading cycles are divided in two groups: pre- and post-yield lateral displacement phases. The first loading phase consists of 3 repetitions of seven targeted symmetrical displacements of 1/20 Δ_y, 1/10 Δ_y, 1/5 Δ_y, 3/10 Δ_y, 2/5 Δ_y and, 1/2 Δ_y to reach the yield displacement Δ_y. Thereafter, two repetitive cycles are imposed with displacement increments of 0.5 Δ_y until 5 Δ_y. In this is study, the analyses continued to failure.

The models for SWS-R and SWN-R were validated based on preliminary analyses of the original wall models shown in Fig. 9 (a) against experimental testing. The original models predicted similar deterioration as that observed in the visual inspection of the original walls after testing, in terms of concrete spalling and crack pattern, along with rupturing of the steel reinforcement. The peak lateral strength and displacement capacity

for Wall SWR was overestimated by 14%. Model SWN overestimated the lateral capacity by less than 10%. The overestimation of the predicted response of the original walls was considered satisfactory.

5. Results

The repair materials were engaged in the FEM models of the repaired walls, while the models retained the residual state from the preliminary analyses of the original walls. Following the same loading protocol, the repaired models were analyzed. Fig. 10 (a) and (b) present the predicted lateral load-drift ratio responses of the repaired walls SWS-R and SWN-R, respectively.

The yield, peak and ultimate points in Fig 10 were established for the positive direction based on the reduced stiffness equivalent elasto-plastic method [36]. Note that the ultimate point is based on a 20% reduction in the lateral load capacity or the displacement cycle prior to fracturing of the reinforcement. The numerical model for SWS-R experienced a peak load of 271.8 kN at a displacement of 35.5 mm (1.5% drift). The yield point corresponded to a load of 257.4 kN and a displacement of 15.8 mm (0.66% drift). The behavior of SWN-R was enhanced, sustaining a peak load of 285.4 kN at a displacement of 94.8 mm (4% drift). Owing to the lower modulus of elasticity of the Nitinol bars, the SMA-reinforced wall experienced yielding at 263.7 kN and 31.6 mm (1.32% drift). It is evident that the wall with ECC, and in combination with SE-SMA longitudinal reinforcement, enhanced the overall behavior. The ductile properties of this novel concrete are more pronounced in Wall SWN-R due to the self-centering capacity of the SMA bars. Global failure of Wall SWS-R occurred at 2.3% drift in comparison to 3.8% drift for Wall SWN-R.

With increasing lateral displacements in the post-peak phase, the strength of Wall SWS-R degrades. In contrast, SWN-R experienced gradual increase in lateral load with increasing lateral displacements. The load-displacement response of SWS-R presented wide hysteretic loops with a residual displacement of 23.6 mm (1% drift) following the 2.5% drift cycle. The combination of ECC with the SE-SMA bars resulted in the pinching of the hysteresis loops of Wall SWN-R, with a reduction of the residual displacement by 48% for the same 2.5% drift.

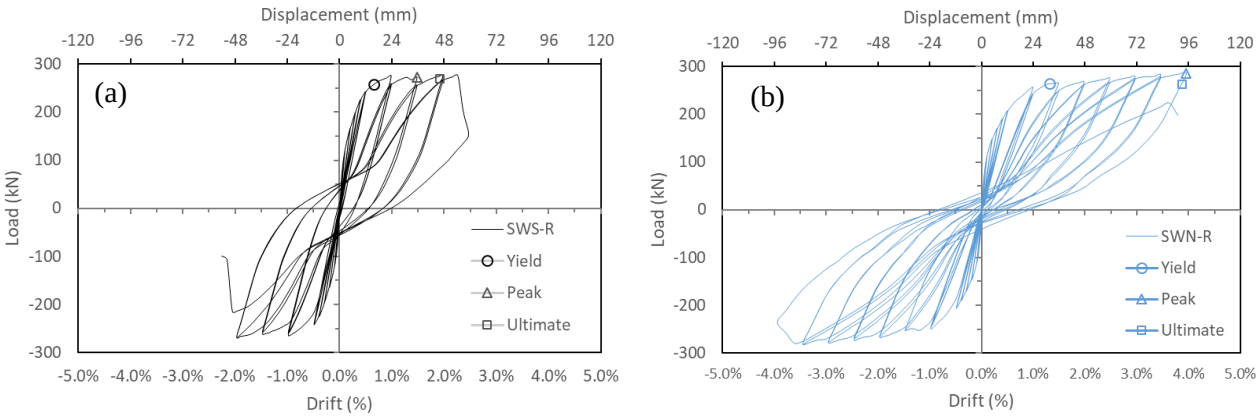

Fig. 10 – Lateral load-displacement responses: (a) Wall SWS-R; (b) Wall SWN-R

Fig. 11 depicts the lateral load-drift response and the stiffness degradation. Both walls experienced a similar behavior with slightly higher lateral load attained by Wall SWS-R up to 2% drift, after which a sudden decay in strength leading to failure at 2.5% drift (60 mm) was realized. Wall SWN-R was able to sustain lateral loading at higher levels of displacements. Furthermore, as illustrate in Fig. 11 (b), Wall SWN-R experienced a higher peak secant stiffness (68.3×10^3 kN/mm) in comparison to SWN-R (60.1×10^3 kN/mm), attributed to the presence of steel rebars in the boundary region with a higher modulus of elasticity than the SE-SMA bars in Wall SWN-R. At 2% drift, both walls experienced comparable stiffness.

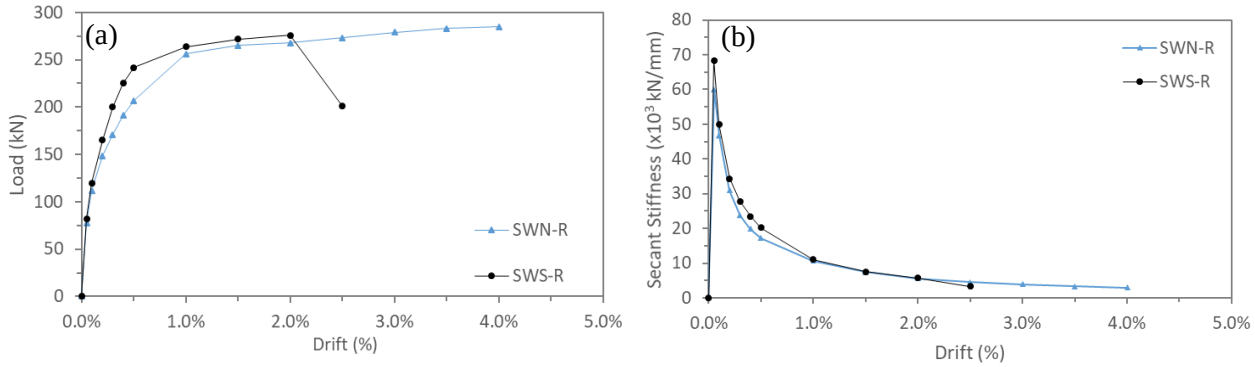

Fig. 11 – (a) Lateral load-drift responses; (b) Secant stiffness-drift degradation

Fig. 12 shows the predicted crack patterns at 2.5% and their respective dissipated energies. Wall SWS-R (Fig. 12 (a)) experienced wide spread flexural-shear cracks in the plastic hinge. Furthermore, severe concrete crushing and loss of the concrete cover was captured at an elevation of 300 mm from the base of the wall. Wall SWN-R (Fig. 12 (b)) experienced milder deterioration. In both walls, the conventional concrete located above the plastic hinge region suffered flexural cracking due to its low tensile strength. Each wall developed a major flexural crack adjacent to the termination of the starter bars that controlled their overall behavior.

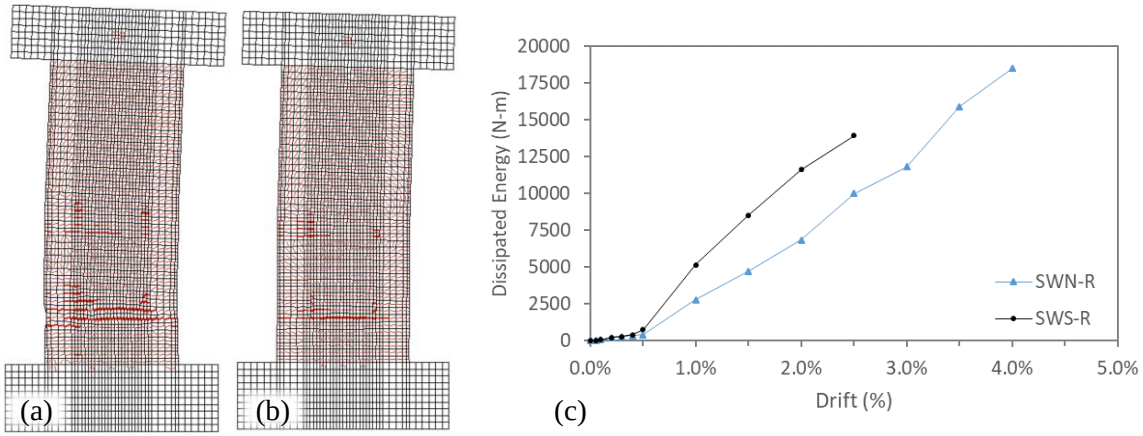

Fig. 12- Predicted crack pattern at 2.5% drift for: (a) SWS-R and (b) SWN-R; (c) Energy dissipation-drift

Wall SWN-R dissipated 28.5% less energy than Wall SWS-R at 2.5% drift. The recovery capacity of the SMA bars along with the high strain capacity of the ECC resulted in pinching of the hysteresis loops and a reduction in the energy dissipation. Conversely, the strain hardening and plastic response of the steel reinforcement in Wall SWS-R at this stage promoted wider hysteresis loops and therefore a higher dissipation of energy. Failure of walls occurred due to rupturing of the steel reinforcement within the plastic hinge area, in the boundary regions for Wall SWS-R and in the web for Wall SWN-R. Note that the SMA bars in the boundary zones of Wall SWN-R remained intact.

Fig. 13 depicts the displacement recovery of the walls. Wall SWN-R fully recovered from drifts of up to 0.5% (12mm), whereas Wall SWS-R fully recovered from 0.2% drifts (4.8mm). At 2.5% drift, the repaired SMA wall recovered 88% of the top lateral displacement, while Wall SWS-R recovered 54% of the displacement.

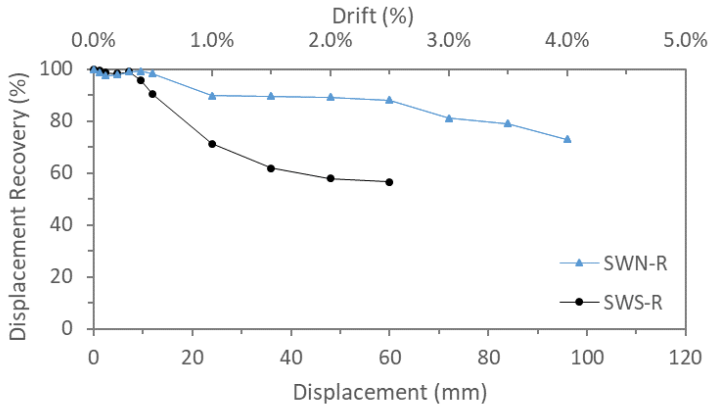

Fig. 13 – Displacement recovery capacity

6. Conclusions

This paper focused on studying the behavior, under reverse cyclic loading, of reinforced concrete shear walls with Shape Memory Alloys (SMAs) and Engineered Cementitious Composite (ECC) within the plastic hinge region. The following conclusions are drawn from this study:

1. The use of ECC as a repairing material is an adequate innovative solution to improve the overall behavior of shear walls resulting in high stiffness and ductility.
2. Both walls failed at a similar lateral load capacity of approximately 280 kN, however at two different drifts: 4% for SWN-R and 2.5% for SWS-R. The wall containing Nitinol SMA bars (SWN-R) was capable of recovering up to 88% of top lateral displacement when subjected to drift of 2.5%.
3. A major flexural crack adjacent to the termination of the starter bars controlled the behavior of both walls. Wall SWN-R provided a more ductile behavior with a significant recovery of cracking in comparison to Wall SWS-R at 2.5%.
4. The addition of starter bars at the base of the walls controlled the rocking/sliding experienced by the original walls.
5. Failure in both walls was governed by the yielding of the longitudinal steel reinforcing bars located in the plastic hinge region; in the boundary zones for SWS-R and in the web for SWN-R.

7. References

[1] S. Mahin, “Sustainable Design Considerations in Earthquake Engineering,” *14th World Conf. Earthq. Eng.*, 2008.
[2] C. Eurocode, “8: Design of structures for earthquake resistance—Part 1: General rules, seismic actions and rules for buildings (EN 1998-1: 2004),” *Eur. Comm. Norm. Brussels*, 2004.
[3] 441 ACI Committee, “441R-96: Report on High-Strength Concrete Columns,” *Tech. Doc.*, 1996.
[4] D. . Lagoudas, *Shape Memory Alloys - Modeling and Engineering Applications*. 1989.
[5] B. Mas, A. Cladera, and C. Ribas, “Fundamentos y aplicaciones piloto de las aleaciones con memoria de forma para su utilización en ingeniería estructural,” *Hormigón y Acero*, 2016.
[6] A. Abdulridha and D. Palermo, “Behaviour and modelling of hybrid SMA-steel reinforced concrete slender shear wall,” *Eng. Struct.*, 2017.
[7] A. E. Naaman and H. W. Reinhardt, “Proposed classification of HPFRC composites based on their tensile response,” *Mater. Struct. Constr.*, 2006.
[8] E. H. Yang and V. C. Li, “Tailoring engineered cementitious composites for impact resistance,” *Cem. Concr. Res.*, 2012.
[9] M. Sahmaran, M. Li, and V. C. Li, “Transport properties of engineered cementitious composites under chloride exposure,” *ACI Mater. J.*, 2007.
[10] B. S. Mohammed, M. F. Nuruddin, M. Aswin, N. Mahamood, and H. Al-Mattarneh, “Structural Behavior of Reinforced Self-Compacted Engineered Cementitious Composite Beams,” *Adv. Mater. Sci. Eng.*, 2016.
[11] M. Ali El-Sayed Mahmoud Ali, “Tensile and Impact Behaviour of Shape Memory Alloy Fibre Reinforced

Engineered Cementitious Composites," University of Western Ontario, 2017.
[12] M. A. E. M. Ali, A. M. Soliman, and M. L. Nehdi, "Hybrid-fiber reinforced engineered cementitious composite under tensile and impact loading," *Mater. Des.*, 2017.
[13] M. M. Sherif, E. M. Khakimova, J. Tanks, and O. E. Ozbulut, "Cyclic flexural behavior of hybrid SMA/steel fiber reinforced concrete analyzed by optical and acoustic techniques," *Compos. Struct.*, 2018.
[14] J. Pereiro-Barceló, J. L. Bonet, B. Cabañero-Escudero, and B. Martínez-Jaén, "Cyclic behavior of hybrid RC columns using High-Performance Fiber-Reinforced Concrete and Ni-Ti SMA bars in critical regions," *Compos. Struct.*, 2019.
[15] M. Mena and D. Palermo, "Numerical modelling of slender superelastic-shape memory alloy reinforced concrete shear walls" in *CSCE Fredericton Annual Conference*, 2018, p. 11.
[16] M. Morcos and D. Palermo, "SMA-Reinforced Concrete Shear Walls Subjected to Reverse Cyclic Loading," in *SMAR 2019 - Fifth Conference on Smart Monitoring, Assesment and Rehabilitation of Civil Structures*, 2019.
[17] Canadian Standards Association, "CSA A23.3-04 Design of Concrete Structures." Rexdale, Canada, 2004.
[18] Fema 461, "Interim Testing Protocols for Determining the Seismic Performance Characteristics of Structural and Nonstructural Components," *Appl. Technol. Counc.*, 2007.
[19] F. J. Vecchio and M. P. Collins, "The Modified Compression Field Theory for reinforced concrete elements subjected to shear," *ACI Struct. J.*, 1986.
[20] F. J. Vecchio, "Disturbed Stress Field Model for Reinforced Concrete: Formulation," *J. Struct. Eng.*, 2000.
[21] P. S. Wong, F. J. Vecchio, and H. Trommels, *VecTor2 and FormWorks user's manual*. 2013.
[22] W. L. Cortés-Puentes and D. Palermo, "Modelling seismically repaired and retrofitted reinforced concrete shear walls," *Comput. Concr.*, 2011.
[23] M. Maciel, D. Palermo, and A. Abdulridha, "Seismic response of SMA reinforced shear walls," in *Conference Proceedings of the Society for Experimental Mechanics Series*, 2016.
[24] S. Ghazizadeh, C. A. Cruz-Noguez, and F. Talaei, "Analytical model for hybrid FRP-steel reinforced shear walls," *Eng. Struct.*, 2018.
[25] S. Popovics, "A numerical approach to the complete stress-strain curve of concrete," *Cem. Concr. Res.*, 1973.
[26] B. D. Scott, R. Park, and M. J. N. Priestley, "Stress-strain behavior of concrete confined by overlapping hoops at low and high strain rates." *J. Am. Concr. Inst.*, 1982.
[27] Kupfer H, Hilsdorf HK, and Rusch H, "Behior of concrete under biaxial stresses," *Am Concr. Inst-J*, 1969.
[28] D. Palermo, "Behaviour and analysis of reinforced concrete walls subjected to reversed cyclic loading," 2002.
[29] G. P. A. G. Van Zijl *et al.*, "Durability of strain-hardening cement-based composites (SHCC)," *Mater. Struct. Constr.*, 2012.
[30] D. Palermo and F. J. Vecchio, "Simulation of cyclically loaded concrete structures based on the finite-element method," *J. Struct. Eng.*, 2007.
[31] M. Seckin, "Hysteretic behavior of cast-in-place exterior beam column sub-assemblies" University of Toronto, 1981.
[32] R. Eligehausen, E. P. Popov, and V. V. Bertero, "Local bond stress-slip relationships of dformed bars under generalized excitations" 1982.
[33] A. Abdulridha, D. Palermo, S. Foo, and F. J. Vecchio, "Behavior and modeling of superelastic shape memory alloy reinforced concrete beams," *Eng. Struct.*, 2013.
[34] F. Vecchio and F. Bucci, "Analysis of repaired reinforced concrete structures," *J. Struct. Eng.*, 1999.
[35] ATC-24, "Guidelines for Cyclic Seismic Testing of Components of Steel Structures. AISI.," 1992.
[36] R. Park, "Ductility evaluation from laboratory and analytical testing," in *Proceedings of the 9th World Conference on Earthquake Engineering, Tokyo-Kyoto, Japan*, 1988.

